


## Periastron shift for a spinning test particle around naked singularities

Sajal Mukherjee\*

*Department of Physical Sciences, IISER-Kolkata, Mohanpur-741246, India*
 (Received 9 February 2018; revised manuscript received 13 April 2018; published 6 June 2018)

In the present article, we investigate the Periastron precession for a spinning test particle moving in nearly circular orbits around naked singularities. We consider two well-known solutions that can produce a spacetime with naked singularity—(a) first, the Reissner-Nordström metric, which is a static charged solution with spherical symmetry, and (b) second, the stationary, axisymmetric Kerr metric. For simplicity, we only consider the motion confined on the equatorial plane in both these cases and solve exactly the Mathisson-Papapetrou equations. In addition, we analytically compute the Periastron precession within the framework of linear spin approximation. The inclusion of the spin parameter modifies the results with nonspinning particles and also reflects some interesting properties of the naked geometries. Furthermore, we carried out a numerical approach without any assumptions to probe the large order spin values. The implication of the spin-curvature coupling in connection with the naked geometries is also discussed.

DOI: [10.1103/PhysRevD.97.124006](https://doi.org/10.1103/PhysRevD.97.124006)

### I. INTRODUCTION

The study of spinning particles is important to understand the evolution of extreme mass ratio binaries [1–3]. Unlike monopole particles, spinning objects are deviated from the geodesic trajectories due to the spin-curvature coupling [4–7]. In 1937, Mathisson studied their motion in the linearized gravity [8], and shortly afterward, Papapetrou derived the orbit equations for these particles in the curved spacetime [9,10]. Following this, Dixon arrived with the equations of motion of extended objects with multipole mass moments [11–13]. These equations have wide and substantial interest in the field of general relativity, spanning from describing trajectories of extended objects [14,15] to modeling a binary system [16]. A Hamiltonian description for these particles is given in Refs. [17,18]. The notion of spinning particles may provide a better understanding to model the behavior of compact objects, such as a black hole or star, around a massive black hole. A similar situation may be found at the center of most of the galaxies, including our own Galaxy with a supermassive black hole at its center named Sgr A\* [19,20].

In this work, we shall explicitly study the motion of these particles in a curved background and be primarily concerned with the Periastron precession on the equatorial plane. We assume that the orbits are nearly circular and the radial frequency ( $\Omega_r$ ) is not equal to the orbital frequency ( $\Omega_\phi$ ); hence, the precession becomes nonzero. Considering our own Solar System, the planets precess due to the perturbation from nearby planets or the quadrupole potential from Sun. These effects have been studied in

Refs. [21,22]. But for the planet Mercury, dominant contribution comes from the relativistic effects, and tools of general relativity become essential to explain it appropriately [23]. According to the Einstein's theory of general relativity, the generic elliptical orbits are not closed in the presence of gravity. This primarily suggests that the particle would never come back to its initial position after a orbital period. In the case of a geodesic trajectory, this precession can be easily computed. However, for a spinning particle, it is a nontrivial job [24]. For spinning black hole binaries, the Periastron advance is computed in Ref. [25] for quasircular orbits by combining both numerical relativity and the effective one body approach. A similar finding by adapting post-Newtonian approximation can be found in Ref. [26]. Relevant studies for nonspinning binaries are shown in Ref. [27]. We refer our readers to Refs. [28–31] for detailed discussion on the effects of spin in a binary system.

In the present context, we consider a spinning test particle orbiting in a nearly circular trajectory while the background spacetime consists of a naked singularity. We explicitly solve the exact Mathisson-Papapetrou equations and analytically compute the difference between  $\Omega_r$  and  $\Omega_\phi$  up to terms linear in spin. In addition, to accommodate quadratic spin dependence, numerical tools have also been used. The absence of the event horizon will allow us to investigate the effect of spin-curvature coupling on the periastron precession close to singularity. We consider two solutions of Einstein-Maxwell field equations that can provide a naked singularity at a certain limit. First is the Reissner-Nordström spacetime, and in this case, the horizon does not exist for the  $Q > M$  limit, where  $M$  and  $Q$  are the mass and charge of the spacetime respectively. This is called the naked Reissner-Nordström spacetime or an

\*sm13ip029@iiserkol.ac.in

overcharging geometry. On the other hand, a similar situation may arise in the case of a Kerr geometry for  $a > M$ , with a the angular momentum of the spacetime. It is called an over-spinning geometry or Kerr superspinor. Naked geometries have gathered intensive attention in recent times due to their interesting properties [32–34]. Even if these objects are highly transient in nature [35], they are suggested to be a promising source of high energy particles in the Universe [36]. A study on the stability analysis of these geometries can be found in Ref. [37]. Though it is true that they have some pathological behavior such as geodesic unpredictability or causality violation [38], they might be astrophysically important and worth exploring [39,40]. We study the effects of these geometries on the motion of a spinning particle specifically in connection with the periastron precession.

The rest of the article is organized as follows. In Sec. II, we shall start with the evolution equations for a spinning particle and discuss several properties of their motion. In Sec. III, we derive the bound circular orbits of a spinning particle in overspinning and overcharging geometry. Section IV is devoted to studying the periastron shift for these orbits on the equatorial plane. Later on in Sec. V, we provide a numerical example for periastron precession in both the geometries for large spin values. Finally, we shall close the article with concluding remarks in Sec. VI.

Throughout the text, we have used the units with  $c = G = 1$  and the metric signature  $(-, +, +, +)$ .

## II. SPINNING PARTICLE IN A GRAVITATIONAL FIELD

The Mathisson-Papapetrou equations [8,9] are given as

$$\begin{aligned}\dot{P}^a &= -\frac{1}{2}R^a{}_{bcd}\mathcal{U}^b S^{cd}, \\ \dot{S}^{ab} &= P^a\mathcal{U}^b - P^b\mathcal{U}^a,\end{aligned}\quad (1)$$

where  $P^a$  defines the 4-momentum,  $S^{ab}$  is the antisymmetric spin tensor, and  $\mathcal{U}^a$  is the four-velocity of the spinning particle. The spin tensor  $S^{ab}$  is essentially related to the structure of the pole-dipole particle, while we have neglected other higher moments. It should be noted that the above equations are not sufficient alone to determine the complete trajectory of a spinning particle. So, further conditions are essential to specify its motion. For a unique choice of the center of mass of the particle, we may employ the Tulczyjew-Dixon spin supplementary condition (SSC) [41], which is given as

$$S^{ab}P_b = 0. \quad (2)$$

This SSC certainly conserves the dynamical mass ( $\mu$ ) of the spinning body [42], and we may now define a normalized momentum  $\mathcal{V}^a$  as

$$\mathcal{V}^a = P^a/\mu; \quad \mathcal{V}^a\mathcal{V}_a = -1. \quad (3)$$

It is important to note that the four-velocity,  $\mathcal{U}^a$ , is not normalized in general when the supplementary condition is given as Eq. (2). So, an additional constraint on the 4-velocity is required to show that the particle is timelike,

$$\mathcal{U}^a\mathcal{U}_a < 0. \quad (4)$$

For simplicity, we may choose [43]

$$\mathcal{U}^a\mathcal{V}_a = -1. \quad (5)$$

Also, for convenience, we replace the spin tensor  $S^{ab}$  with a spin 4-vector  $S^a$ ,

$$S^{ab} = \frac{1}{\sqrt{-g}}\epsilon^{abcd}S_c P_d, \quad (6)$$

where  $g$  is the determinant of the metric. Form Eqs. (1)–(5), one can establish a relation between four-velocity and the momentum,

$$\mathcal{U}^a - \mathcal{V}^a = \frac{S^{ab}R_{bcdf}\mathcal{V}^c S^{df}}{2(\mu^2 + \frac{1}{4}R_{pqrs}S^{pq}S^{rs})}. \quad (7)$$

Furthermore, the symmetries of the spacetime will contribute to additional conserved quantities, and due to the nonzero spin, they may include some spin-dependent terms. For example, with a given killing vector field  $K^a$ , the conserved quantity is given as [44,45]

$$C = K^a P_a - \frac{1}{2}S^{ab}K_{a;b}. \quad (8)$$

It should be noted that, unlike energy ( $-P_t$ ) or angular momentum ( $P_\phi$ ),  $C$  defines a different quantity which depends on spin. For example, when  $K^a = \xi^a$ , a timelike killing vector, the energy is given as  $E_{\text{infy}} = -\xi^a P_a$ , which is not conserved in the presence of spin. But the conserved quantity is given as

$$C_t = -E_{\text{infy}} - \frac{1}{2}S^{ab}\xi_{a;b}. \quad (9)$$

So, for spinning particles, we define  $E = -C_t$  and  $J_z = C_\phi$ , and these reduce to the well-defined energy ( $\xi^a P_a$ ) and angular momentum ( $\eta^a P_a$ ) for a geodesic, where  $\eta^a$  is the spacelike killing vector field.

### A. Motion in the Reissner-Nordström spacetime

In this subsection, we shall discuss the motion of a spinning particle in the Reissner-Nordström spacetime. The metric element is given as

$$ds^2 = -\left(1 - \frac{2M}{r} + \frac{Q^2}{r^2}\right)dt^2 + \frac{dr^2}{\left(1 - \frac{2M}{r} + \frac{Q^2}{r^2}\right)} + r^2(d\theta^2 + \sin^2\theta d\phi^2), \quad (10)$$

where  $M$  and  $Q$  are the mass and charge parameter of the spacetime respectively. In addition to that, as the system is endowed with the spherical symmetry, we shall confine our discussion only on the equatorial plane without losing any generality. In this case, the spin vector remains perpendicular to the orbital plane, and only the z-component of the vector,  $S^z = -rS^\theta$ , survives. The total spin is given as  $|S| = \sqrt{S^\theta S_\theta} = |S^z|$ , and this is a constant of motion. By using Eqs. (1)–(7), one can write down the relation between the 4-momentum and the four-velocity as

$$\begin{aligned} \mathcal{U}^t &= \frac{\mathcal{V}^t}{N} \left(1 - \frac{MS^2}{r^3} + \frac{S^2 Q^2}{r^4}\right), \\ \mathcal{U}^r &= \frac{\mathcal{V}^r}{N} \left(1 - \frac{MS^2}{r^3} + \frac{S^2 Q^2}{r^4}\right), \\ \mathcal{U}^\phi &= \frac{\mathcal{V}^\phi}{N} \left(1 + \frac{2MS^2}{r^3} - \frac{3S^2 Q^2}{r^4}\right), \\ N &= 1 + \frac{S^2}{r^4} [(Q^2 - Mr) + (4Q^2 - 3Mr)\mathcal{V}^\phi \mathcal{V}_\phi]. \end{aligned} \quad (11)$$

The above expressions can be used along with Eq. (8) to produce the equations of motion:

$$\begin{aligned} (\Sigma_{srn} \Lambda_{srn} \mathcal{U}^r)^2 &= \left(Er^2 + \frac{J_z S}{r^2} \{Q^2 - Mr\}\right)^2 \\ &\quad - \Delta_{RN} \left\{ (J_z - ES)^2 + \frac{\Sigma_{srn}^2}{r^2} \right\}, \\ (\Sigma_{srn} \Lambda_{srn} \mathcal{U}^t) &= \frac{1}{\Delta_{RN}} [Er^4 + J_z S (Q^2 - Mr)], \\ (\Sigma_{srn} \Lambda_{srn} \mathcal{U}^\phi) &= (J_z - ES) \left\{ 1 + \left(3MS^2 - \frac{4Q^2 S^2}{r}\right) \frac{1}{r \Sigma_{srn}} \right\}. \end{aligned} \quad (12)$$

Here,  $E$  and  $J_z$  are defined as two conserved quantities related to timelike and spacelike symmetries of the spacetime, as described in the last section. The quantity  $S$  represents the total spin of the particle. We define  $\Sigma_{srn}$  and  $\Lambda_{srn}$  as

$$\begin{aligned} \Sigma_{srn} &= r^2 \left(1 - \frac{MS^2}{r^3} + \frac{Q^2 S^2}{r^4}\right), \\ \Lambda_{srn} &= 1 + \frac{S^2}{\Sigma_{srn}^3} (4Q^2 - 3Mr)(J_z - ES)^2. \end{aligned} \quad (13)$$

In addition, to retain the timelike property of the spinning particle, one has to ensure  $\mathcal{U}^a \mathcal{U}_a < 0$ , and this will give further constraints on its motion.

## B. Motion in the Kerr spacetime

The Kerr metric, written in the Boyer-Lindquist coordinates, is given by

$$ds^2 = -\frac{(\Delta - a^2 \sin^2\theta)}{\Sigma} dt^2 + \frac{\Sigma}{\Delta} dr^2 + \Sigma d\theta^2 - \frac{4Mar \sin^2\theta}{\Sigma} + \frac{(r^2 + a^2)^2 - \Delta a^2 \sin^2\theta}{\Sigma} \sin^2\theta d\phi^2, \quad (14)$$

where  $M$  and  $a$  are the mass and angular momentum parameter of the spacetime and  $\Delta = r^2 - 2Mr + a^2$ ,  $\Sigma = r^2 + a^2 \cos^2\theta$ . Saijo *et al.* derived the equation of motion of a spinning particle on the equatorial plane of a Kerr black hole [43,46]. These equations are given as

$$\begin{aligned} (\Sigma_s \Lambda_s \mathcal{U}^r)^2 &= P_s^2 - \Delta \left( \frac{\Sigma_s^2}{r^2} + \{J_z - (a+S)E\}^2 \right), \\ (\Sigma_s \Lambda_s \mathcal{U}^t) &= a \left( 1 + \frac{3MS^2}{r \Sigma_s} \right) \{J_z - (a+S)E\} + \frac{r^2 + a^2}{\Delta} P_s, \\ (\Sigma_s \Lambda_s \mathcal{U}^\phi) &= \left( 1 + \frac{3MS^2}{r \Sigma_s} \right) \{J_z - (a+S)E\} + \frac{a}{\Delta} P_s, \end{aligned} \quad (15)$$

where  $P_s$ ,  $\Sigma_s$ , and  $\Lambda_s$  are given as

$$\begin{aligned} P_s &= E \left( r^2 + a^2 + aS + \frac{aSM}{r} \right) - \left( a + \frac{MS}{r} \right) J_z, \\ \Sigma_s &= r^2 (1 - MS^2/r^3), \\ \Lambda_s &= 1 - \frac{3MS^2 r}{\Sigma_s^3} \{J_z - (a+S)E\}^2. \end{aligned} \quad (16)$$

Similar to the spherically symmetric case in Sec. II A, the quantity  $S$  represents the total spin acting only in the  $z$  direction,  $S = (0, 0, 0, S^z)$ . This is either parallel ( $S > 0$ ) or antiparallel ( $S < 0$ ) to the rotational axis of the geometry. Further, by using Eqs. (15) and (16), one can rewrite the timelike condition as given in Eq. (4),

$$r^5 \left( 1 - \frac{MS^2}{r^3} \right)^4 > 3MS^2 \left( 2 + \frac{MS^2}{r^3} \right) \{J_z - (a+S)E\}^2. \quad (17)$$

The above equation determines the closest interaction of a spinning particle with the black hole. For the  $S = 0$  limit, it is trivially satisfied, and no additional constraint is applied on its motion.

## III. CIRCULAR ORBITS IN NAKED GEOMETRIES

In this section, we briefly study the existence of circular orbits and carry out their stability analysis in both Reissner-Nordström and Kerr spacetime. For analytical convenience, we only consider the equatorial plane. The necessary conditions for a circular orbit to exist are given as

$$\dot{r}^2 = V_{\text{eff}}(r) = 0, \quad \ddot{r} = \frac{1}{2} \frac{dV_{\text{eff}}(r)}{dr} = 0. \quad (18)$$

Here,  $V_{\text{eff}}$  is defined as the radial effective potential, and a dot defines a derivative with respect to the affine parameter  $\tau$ . The above equations, in principle, can be solved to compute the energy and angular momentum of a particle.

### A. Reissner-Nordström spacetime

Before delving into the rotating geometry, let us first discuss the circular orbits in Reissner-Nordström spacetime. We shall start by solving the Eq. (18) to compute  $E$  and  $J_z$  in both the geodesic and spinning cases. In the spinning case, we approximate the results only up to the linear order in spin. The minima of the energy and angular momentum will give the innermost stable circular orbit (ISCO) for different sets of parameters such as  $Q$  or  $S$  [47].

#### 1. Geodesic motion

A circular geodesic in the Reissner-Nordström geometry has energy  $E_{\text{Geo}}^{\text{RN}}$  and angular momentum  $J_{\text{Geo}}^{\text{RN}}$ :

$$\begin{aligned} (J_{\text{Geo}}^{\text{RN}})^2 &= r^2 \frac{Mr - Q^2}{r^2 + 2Q^2 - 3Mr}, \\ E_{\text{Geo}}^{\text{RN}} &= \frac{r^2 - 2Mr + Q^2}{r\sqrt{r^2 - 3Mr + 2Q^2}}. \end{aligned} \quad (19)$$

The above equation would immediately suggest that  $r^2 - 3Mr + 2Q^2 > 0$ . It essentially indicates that no circular orbit could exist for a timelike particle with  $r^2 - 3Mr + 2Q^2 \leq 0$  while  $r^2 - 3Mr + 2Q^2 = 0$  describes the photon orbit. The other constraint  $Mr > Q^2$  only appears due to the geometry of the considered spacetime and is trivially satisfied in the case of a Schwarzschild spacetime.

The ISCO is determined by  $V_{\text{eff}}''(r) = 0$ , where a prime defines a derivative with respect to  $r$ . The ISCOs can be further subcategorized as the following:

- (i) Case A: For  $5M^8Q^4 - 9M^6Q^6 + 4M^4Q^8 < 0$  or  $Q < Q_c = \sqrt{5}M/2$ , one can show  $V_{\text{eff}}''(r) = 0$  has three solutions,

$$\begin{aligned} r_1 &= 2M \left[ 1 + \sqrt{\{4M^2 - 3Q^2\} \cos\left(\frac{\theta}{3}\right)} \right], \\ r_2 &= 2M \left[ 1 - \sqrt{\{4M^2 - 3Q^2\} \cos\left(\frac{\theta}{3} + \frac{\pi}{3}\right)} \right], \\ r_3 &= 2M \left[ 1 - \sqrt{\{4M^2 - 3Q^2\} \cos\left(\frac{\theta}{3} - \frac{\pi}{3}\right)} \right], \end{aligned} \quad (20)$$

where  $\theta = \tan^{-1}\left(\frac{\sqrt{9M^6Q^6 - 4M^4Q^8 - 5M^8Q^4}}{8M^6 - 9M^4Q^2 + 2M^2Q^4}\right)$ , and the solutions follow the order as  $r_3 < Q^2/M < r_2 < r_1 < \infty$ . This immediately rules out  $r_3$  as  $Mr_3 < Q^2$ , and it is

inconsistent with Eq. (19). For the case with  $r = r_2$ , the reason is a bit involved and can be explained as the following. In the case of naked Reissner-Nordström geometry with  $M < Q < Q_c$ , there can exist two different regions, i.e.,  $Q^2/M < r < r_2$  and  $r_1 < r < \infty$ , where stable circular orbits can exist. But these two domains are separated by a region with instability that is  $r_2 < r < r_1$ , where no stable orbit can exist. In the present context, where we are interested in orbits arriving from spatial infinity, we consider the ISCO is located at  $r = r_1$  and beyond that no stable orbit exists.

- (ii) Case B: In the case for  $Q \geq Q_c$  or  $5M^8Q^4 - 9M^6Q^6 + 4M^4Q^8 \geq 0$ , the ISCO is located at  $r = Q^2/M$ .

### 2. Spinning particle

We now consider the motion of a spinning particle moving in a circular orbit and compute the energy and angular momentum associated with it. The effective radial potential is given by  $V_{\text{eff}}(r, S)$ , which explicitly depends on the spin parameter as given in Eqs. (12) and (13):

$$V_{\text{eff}}(r, S) = \frac{1}{(\Sigma_s \Lambda_s)^2} \left\{ P_s^2 - \Delta \left( \frac{\Sigma_s^2}{r^2} + \{J_z - (a + S)E\}^2 \right) \right\}. \quad (21)$$

Hence, similar to the  $S = 0$  case, one can solve Eq. (18) with the above potential up to terms linear in spin. The energy and angular momentum are given as

$$\begin{aligned} E^{(1,2)} &= \frac{\Delta_{\text{RN}}}{r\sqrt{\alpha}} \pm \frac{S}{2r^3} \left\{ 2\sqrt{\beta\alpha} - \Delta_{\text{RN}} \sqrt{\beta} \frac{\Delta_{\text{RN}} + \alpha - 4\beta + Q^2}{\alpha^{3/2}} \right\}, \\ J_z^{(1,2)} &= \mp \frac{r\sqrt{\beta}}{\sqrt{\alpha}} + \frac{S\Delta_{\text{RN}}(\Delta_{\text{RN}} + \alpha - 4\beta + Q^2)}{2r\alpha^{3/2}}, \end{aligned} \quad (22)$$

where  $\Delta_{\text{RN}} = r^2 - 2Mr + Q^2$ ,  $\alpha = r^2 - 3Mr + 2Q^2$ , and  $\beta = Mr - Q^2$ , with  $M$  and  $Q$  representing their usual meanings. Here,  $E^{(i)}$  is defined as the energy corresponding to angular momentum  $J_z^{(i)}$ , for  $i = 1$  to  $2$ . In Figs. 1(a)–1(d), both  $E^{(i)}$  and  $J^{(i)}$  are shown for various charge parameters  $Q$ , while the spin of the particle is fixed at  $S = 0.1M$ . To compute the ISCO, one has to solve  $V_{\text{eff}}''(r, S) = 0$  along with the necessary conditions for circular orbit as given in Eq. (18). Similar to the geodesic case with  $0 < Q \leq M$ , the ISCO appears at  $r = r_1^S$ , which is now a function of  $S$ . But whenever  $M < Q < Q_c^S$ , two disconnected stable regions appear within  $Q^2/M < r < r_2^S$  and  $r_1^S < r < \infty$ . In this case,  $Q_c^S$  is the critical value of the charge parameter of the spacetime beyond which these two stable regions merge and the ISCO exists at  $r = Q^2/M$ . For  $S = 0.04M$ ,

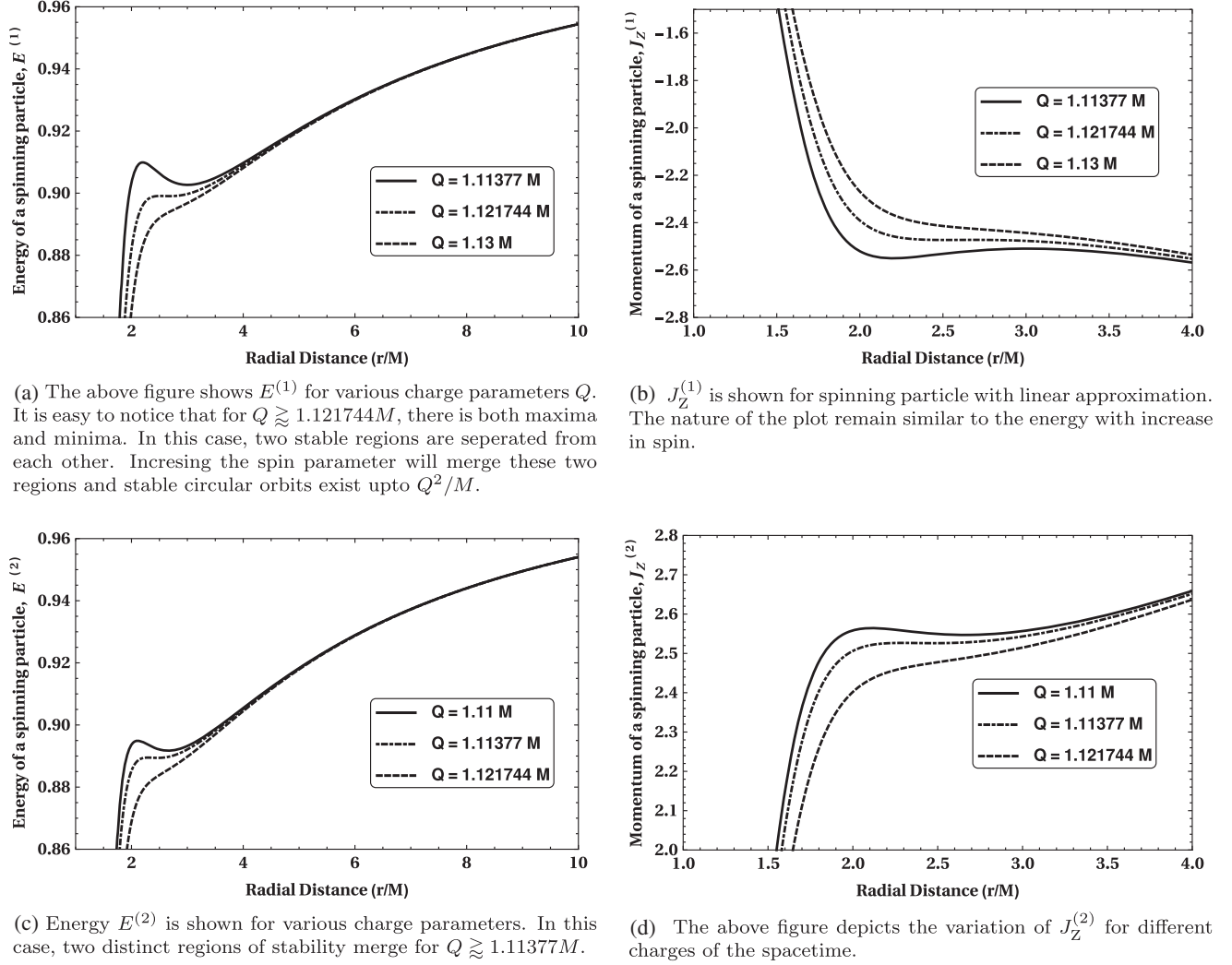


FIG. 1. The energy and angular momentum of a spinning particle are shown in the Reissner-Nordström spacetime. The spin parameter is set at  $S = 0.1M$ .

the  $Q_c^S \approx 1.1188402M$ , while at  $S = -0.04M$ ,  $Q_c^S$  becomes  $1.1172409M$ .

## B. Kerr spacetime

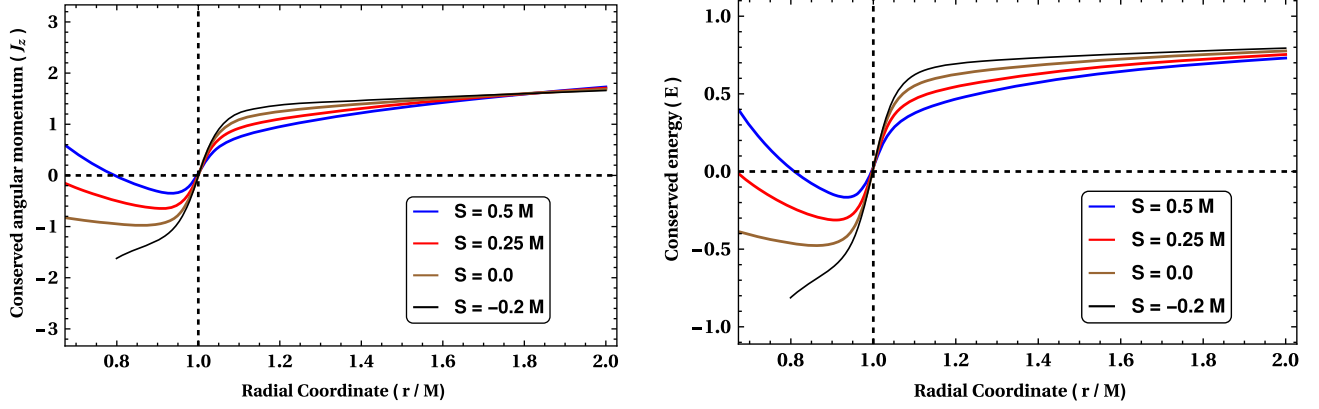
The motion of geodesic trajectories is well studied in the Kerr spacetime both in the equatorial and nonequatorial planes [48,49]. In addition to that, the various aspects of naked Kerr spacetime or Kerr superspinners are also explored in connection with these motions [50,51]. Hence, we shall

only concentrate on the motion of spinning particles and study their orbits.

The motion of a spinning particle, as we described earlier, depends on the choice of a reference point and is more involved than the geodesics. Due to this, we shall carry out an approximate expression for both energy and angular momentum, which is valid only up to the linear order in spin. These are written as [46]

$$\begin{aligned}
 E &= \frac{r^{3/2} - 2Mr^{1/2} \mp aM^{1/2}}{r^{3/4}(r^{3/2} - 3Mr^{1/2} \mp 2aM^{1/2})^{1/2}} + \frac{SE^S}{2r^{11/4}(r^{3/2} - 3M\sqrt{r} - \mp 2a\sqrt{M})^{3/2}}, \\
 J_Z &= \frac{\mp M^{1/2}(r^2 \pm 2aM^{1/2}r^{1/2} + a^2)}{r^{3/4}(r^{3/2} - 3Mr^{1/2} \mp 2aM^{1/2})^{1/2}} + \frac{SJ^S}{2r^{11/4}(r^{3/2} - 3Mr^{1/2} \mp 2aM^{1/2})^{3/2}},
 \end{aligned} \tag{23}$$





(a) Angular momentum is shown for various spin values. For nearly overspinning geometry, the momentum is close to zero at  $r = M$ . It changes its sign from positive to negative at  $r \rightarrow M$ . The Kerr angular momentum is fixed at  $a = 1.001M$ .

(b) The conserved quantity  $E$  is shown for various spin values. Like  $J_z$ , at  $r \rightarrow M$ ,  $E$  goes to zero and changes its sign from positive to negative. The Kerr angular momentum is fixed at  $a = 1.001M$ .

FIG. 2. Energy and angular momentum of a spinning particle in Kerr geometry.

where

$$\begin{aligned}
 J^S &= 2r^5 - 13Mr^4 \mp 9aM^{1/2}r^{7/2} + 18M^2r^3 \\
 &\quad \pm 21aM^{3/2}r^{5/2} + 2a^2Mr^2 \mp 3a^3M^{1/2}r^{3/2} \\
 &\quad + 4a^2M^2r \pm 7a^3M^{3/2}r^{1/2} + 3a^4M, \\
 E^S &= M(a \pm \sqrt{Mr})(r^2 + 3a^2 \pm 4a\sqrt{Mr}). \quad (24)
 \end{aligned}$$

Now, in principle, there are two total solutions to  $E$  and  $J_z$ , which can be easily interpreted from the above equations. But we shall only consider the solutions which can describe the motions arriving from infinity as well as close to  $r = M$ . This only appears when the denominator is given as  $r^{3/2} - 3Mr^{1/2} + 2aM^{1/2}$ . The expression  $r^{3/2} - 3Mr^{1/2} + 2aM^{1/2} = 0$  never gives a real solution of  $r$  in the overspinning geometry ( $a > M$ ), and both the energy and angular momentum behave regularly in the considered region. In Figs. 2(a)–2(b), energy and angular momentum are shown for a variety of spin parameters. Both of them approach zero at  $r \rightarrow M$  for any numerical value of the spin parameter. It is, in fact, related to a particular consequence of the nearly overspinning Kerr spacetime, i.e.,  $a = \lim_{\epsilon \rightarrow 0} M(1 + \epsilon)$ , while for  $\epsilon \approx \mathcal{O}(1)$ , this is no longer valid.

#### IV. PERIASTRON PRECESSION FOR SPINNING PARTICLES

In this section, we shall discuss the periastron precession related to a spinning particle orbiting in nearly circular orbits. We mainly explore the modification of precession frequency due to the intrinsic momentum of a particle. In addition, we also study the role played by the background metric specifically in connection with the naked geometries. As we have discussed earlier, both of the spacetimes we have considered here, namely the Reissner-Nordström

geometry and Kerr spacetime, can produce a spacetime with naked singularity.

Let us now consider a spinning particle moves in a stable circular orbit with radius  $r = r_0$ , and then it is slightly displaced from its position. It will start to oscillate about  $r_0$  with a frequency  $\Omega_r^2 = -\frac{1}{2} \left( \frac{d^2 V_{\text{eff}}}{dr^2} \right)_{r=r_0}$  and moves in a nearly circular orbit, where  $V_{\text{eff}}$  is defined as the effective radial potential of the particle. In the Newtonian gravity, this will form a closed loop, and  $\Omega_r$  is equal to  $\Omega_\phi = \dot{\phi} = \frac{d\phi}{d\tau}$  [52]. But close to the black hole where relativistic effects are dominant, we have  $\Omega_r \neq \Omega_\phi$ , and their difference is referred to the periastron precession and given as

$$\Omega_P = \Omega_\phi - \Omega_r = \frac{d\phi}{d\tau} - \sqrt{\frac{1}{2} \left( -\frac{d^2 V_{\text{eff}}}{dr^2} \right)}. \quad (25)$$

In the next sections, we shall explicitly use the above expression to compute the periastron precession related to a spinning particle.

#### A. Reissner-Nordström spacetime

In the Reissner-Nordström spacetime,  $\Omega_r$  and  $\Omega_\phi$  can be computed by using Eqs. (22) and (25). They can be approximated up to linear order in spin as

$$\begin{aligned}
 (\Omega_\phi^\mp)^2 &= \frac{1}{r^2} \frac{\beta}{\alpha} \mp S \Delta_{\text{RN}} \sqrt{\beta} \frac{4Q^2 - 3Mr}{r^4 \alpha^2}, \\
 (\Omega_r^\mp)^2 &= \frac{\gamma}{r^4 \alpha} \pm S \frac{\sqrt{\beta} \Delta_{\text{RN}} \delta}{r^5 \alpha^2}, \quad (26)
 \end{aligned}$$

where  $\Delta_{\text{RN}}$ ,  $\alpha$ , and  $\beta$  have the predefined meaning and

$$\begin{aligned}
 \gamma &= -4Q^4 + 9MQ^2r + Mr^2(r - 6M), \\
 \delta &= 8Q^2r - 3M(2Q^2 + r^2). \quad (27)
 \end{aligned}$$

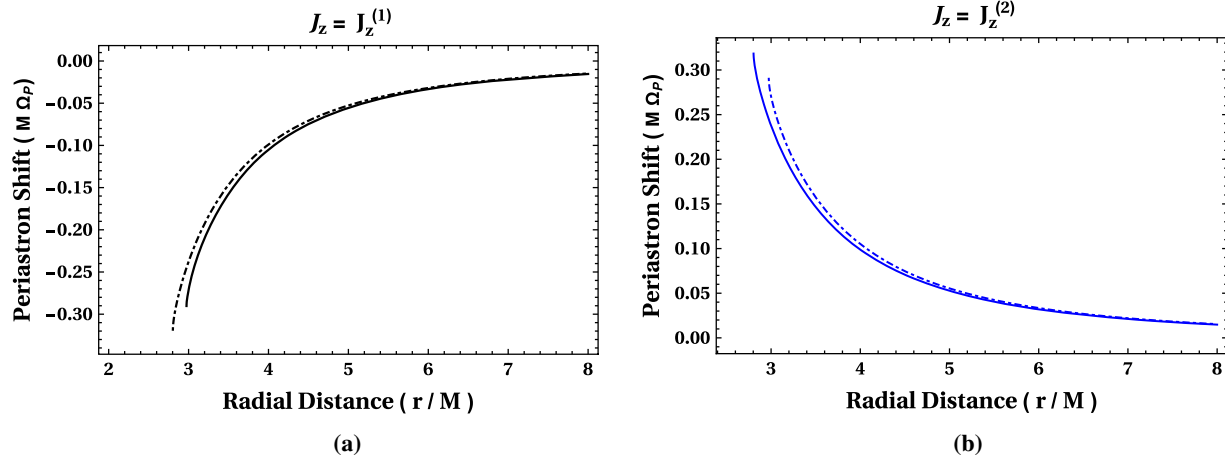


FIG. 3. The periastron shift is shown in a Reissner-Nordström spacetime with the charge parameter,  $Q = 1.11M$ . The straight line is for  $S = 0.04M$ , and the dotted line is for  $S = -0.04M$ . Two regions of stability are disconnected, and the ISCO exists at  $r = r_1^S$ . (a) Periastron precession is shown for  $J_Z = J_Z^{(1)}$  and  $E = E^{(1)}$ . (b) Figure shows the periastron shift with  $J_Z = J_Z^{(2)}$  and  $E = E^{(2)}$ .

It is easy to see that the frequencies diverge at  $\alpha = 0$ , which is the photon orbit. A timelike particle would require infinite energy to move in that orbit. Hence, that scenario is not physically acceptable and is excluded in the text. The periastron shift is shown in Figs. 3 and 4 for different charge parameters in the Reissner-Nordström spacetime, while we fix the spin value at  $S = \pm 0.04M$ . It was suggested earlier in Sec. III A 2 that in a naked Reissner-Nordström geometry there exist two disconnected regions with stable circular orbits when the charge parameter follows  $M < Q < Q_c^S$ . But whenever  $Q \geq Q_c^S$ , these two regions get connected, and a stable circular could exist up to  $r = Q^2/M$ . This can be well understood from Figs. 3 and 4 where we consider two different values of the charge parameter  $Q$  and the consequences change accordingly. For  $Q = 1.11M$ , two stable regions are disconnected by an unstable domain, and as given in Sec. III A 2, the ISCO

exists at  $r = r_1^S$ . This is reflected in the precession frequency as shown in Figs. 3(a) and 3(b). In Fig. 3(a), the precession frequency is computed for  $J_Z = J_Z^{(1)}$ , and the orbits are given with  $\Omega_\phi < 0$ . Hence, the precession frequency is given by  $\Omega_p = -(|\Omega_\phi| - |\Omega_r|)$ . In the case of Fig. 3(b), the orbits are characterized as  $\Omega_\phi > 0$ . We assume the precession is given by  $\Omega_p = (|\Omega_\phi| - |\Omega_r|)$ . A similar convention is used for  $Q = 1.19M$ , as shown in Fig. 4.

It is shown in Fig. 3(a) that  $\Omega_p$  steadily decreases close to the singularity and becomes minimum at  $r = r_1^S$ . Similarly, in Fig. 3(b),  $\Omega_p$  increases and attains a maximum value at  $r = r_1^S$ . In the case of  $Q = 1.19M$ , two separate regions of stability merge, and the ISCO is located at  $Q^2/M$ . Precession frequency reaches a maximum (or minimum) and starts to decrease (or increase) as it moves close to the singularity. It is also important to note that  $\Omega_p$  vanishes at a particular value of

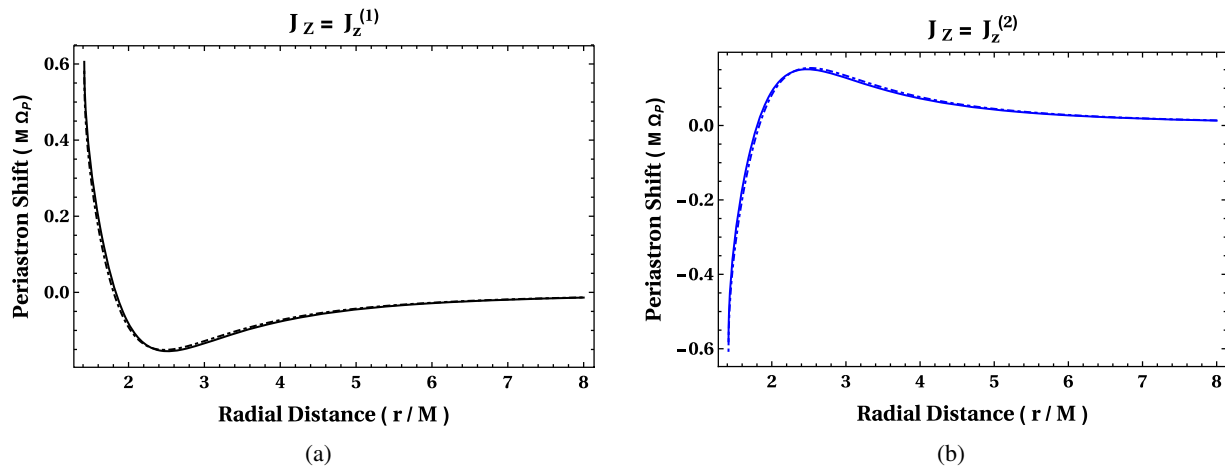


FIG. 4. The figure shows the periastron precession for  $Q = 1.19M$  and  $S = 0.04M, -0.04M$ . In this case, the ISCO exists at  $r = Q^2/M = 1.4161M$ . The straight and dotted lines represent the same significance as in Fig. 3. (a) Precession is shown for  $J_Z = J_Z^{(1)}$  and  $E = E^{(1)}$ . (b) Shift is depicted for  $J_Z = J_Z^{(2)}$  and  $E = E^{(2)}$ .

$r$ , i.e.,  $|\Omega_\phi| = |\Omega_r|$ , and then changes its sign. This phenomenon could be useful to distinguish an overcharging geometry from a black hole. A numerical study to probe the large spin values is carried out in the last section.

In a standard way, the periastron shift can be calculated for  $r \gg M$ :

$$\Omega_p^{(\mp)} = \mp \frac{3M^{3/2} - Q^2/(2\sqrt{M})}{r^{5/2}} - S \left\{ \frac{3M}{r^3} + \frac{12M^2 - 27Q^2/4}{r^4} \right\}. \quad (28)$$

The above equation reduces to the well-defined Perihelion shift for  $S = 0$  and  $Q = 0$ .

## B. Kerr spacetime

Considering the case with Kerr spacetime, we may employ Eqs. (23) and (25) to evaluate the frequencies up to the linear order in spin,

$$\begin{aligned} \Omega_\phi^2 &= \frac{M}{r^{3/2}\eta} + \frac{2FS\sqrt{M}}{\eta^2 r^{3/4}}, \\ \Omega_r^2 &= \frac{M}{r^{7/2}\eta} + \frac{2GS}{r^{7/4}\eta^2}, \end{aligned} \quad (29)$$

where

$$\begin{aligned} F &= \frac{3(a^2M + M(2M - r)r + a\sqrt{Mr}(r - 3M))}{2r^{11/4}}, \\ G &= \frac{3M(\sqrt{Mr} - a)(7a^3M^{1/2} + aM^{1/2}(14M - 5r)r + 5a^2r^{1/2}(r - 4M) + r^{5/2}(r - 2M))}{2r^{15/4}}, \\ \chi &= (-3a^2 + 8a\sqrt{M}\sqrt{r} + r(r - 6M)), \\ \eta &= 2aM^{1/2} + (r - 3M)r^{1/2}. \end{aligned}$$

Similar to the Reissner-Nordström case, one can carry out the approximate expression for periastron shift with the  $r \gg M$  limit:

$$\Omega_p = \left( \frac{3M^{3/2}}{r^{5/2}} - \frac{4aM}{r^3} \right) + S \left\{ -\frac{3M}{r^3} + \frac{3aM^{1/2}}{r^{7/2}} \right\}. \quad (30)$$

## C. Nearly overspinning Kerr spacetime

Here, we consider a nearly overspinning geometry and compute the periastron frequency close to  $r = M$ . This particular limit is maximally efficient in terms of energy extraction from a naked singularity [53,54],

$$a = \lim_{\epsilon \rightarrow 0^+} M(1 + \epsilon). \quad (31)$$

The  $E$  and  $J_z$  can be computed in this limit by using Eq. (23):

$$\begin{aligned} E &= \frac{\sqrt{a - M}(4M^2 + 3aS - MS)}{4\sqrt{2}M^{5/2}}, \\ J &= \frac{\sqrt{a - M}(3a^2S + 2aM(2M + S) + M^2(7S - 4M))}{4\sqrt{2}M^{5/2}}. \end{aligned} \quad (32)$$

It is easily noticeable that both of the above quantities are close to zero for  $a \rightarrow M$ , and it also can be seen from Fig. 2. These expression can be used to compute the periastron frequency up to linear order in spin at  $r = M$ ,

$$\Omega_p \approx \frac{1}{\sqrt{2}} \left( \frac{1}{\sqrt{M}\sqrt{a - M}} - \frac{\sqrt{5M - 3a}}{M^{3/2}} \right) + F(S), \quad (33)$$

where

$$F(S) = \frac{3S}{4\sqrt{2}} \left( \frac{\sqrt{a - M}}{M^{5/2}} + \frac{M^2 + 7a^2 - 8aM}{\sqrt{M}^{7/2}\sqrt{5M - 3a}} \right). \quad (34)$$

The first term in Eq. (33) diverges as  $a$  approaches  $M$ , while  $F(S)$  becomes close to zero in this limit. This essentially suggests that the effect of the spin parameter can be neglected at  $r = M$ , while the spacetime follows Eq. (31). Even if these results are carried out in an approximate framework, the above statement can be extended for large spin values as well. This is explicitly shown in the next section.

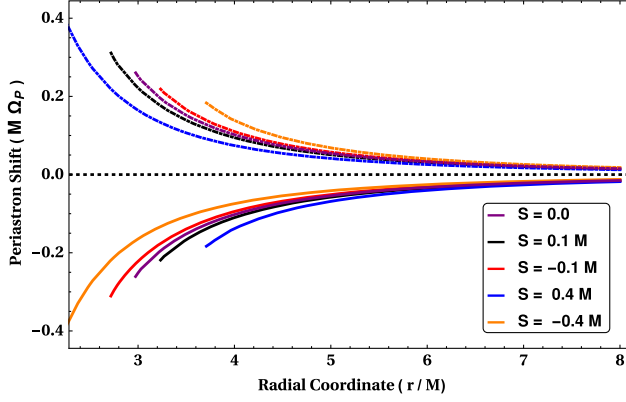
## V. NUMERICAL RESULTS

In this section, we study the numerical aspects of the problem and investigate the behavior in the large spin domain. We start with the Reissner-Nordström geometry and concentrate only on the  $Q > M$  limit. Further, we shall address the Kerr superspinors with  $a > M$ .

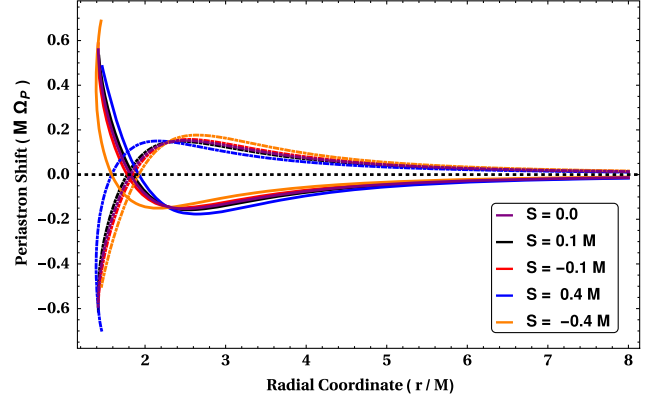
### A. Naked Reissner-Nordström geometry

Here, we investigate the nature of  $\Omega_p$  with two different charge parameters,  $Q = 1.11M$  and  $Q = 1.19M$ . In the first case as shown in Fig. 5(a), two different regions of stability are disconnected, and precession frequency





(a) Figure shows the Periastron shift for  $Q = 1.11M$ . Similar to the spinless case, the charge parameter plays a crucial role. The precession become maximum at the ISCO located at  $r = r_1^S$ .



(b) Precession frequency is shown for  $Q = 1.19M$ . The nature is similar for both spinless and spinning particle. As the charge parameter ( $Q$ ) become more than the critical value ( $Q_c^S$ ), the peak in the frequency appears. It is also important to note that the frequency vanishes at a particular value of  $r$ .

FIG. 5. The precession frequency of a spinning particle in Reissner-Nordström geometry.

reaches a maximum (or minimum) at the ISCO. The situation is similar to the analytical results as shown in Fig. 3. Here, we assume that whenever  $\Omega_\phi > 0$  the precession frequency is given as  $\Omega_p = (|\Omega_\phi| - |\Omega_r|)$ , and for  $\Omega_\phi < 0$ , the frequency becomes  $\Omega_p = -(|\Omega_\phi| - |\Omega_r|)$ . In case of  $Q = 1.19M$ , these two regions get connected, and  $\Omega_p$  attains either a maximum ( $\Omega_\phi > 0$ ) or minimum ( $\Omega_\phi < 0$ ), as shown in Fig. 5(b). It is also instructive to note that the frequency vanishes at a particular value of  $r$  and then changes its sign. This is an interesting and nontrivial feature associated with the naked Reissner-Nordström geometry and easy to understand by examining Eq. (28). For a nonspinning particle at large distance ( $r \gg M$ ), the leading order contribution in  $\Omega_p$  vanishes at  $Q = \sqrt{6}M$  and changes its sign for  $Q \leq \sqrt{6}M$ . This particular limiting value would change whenever one considers a nonzero value of the spin parameter  $S$ . Even if the nature of the precession frequency remains unaffected due to the intrinsic momentum of a particle, there are certain differences that appear at the  $S \neq 0$  limit. For example, as Reissner-Nordström geometry is endowed with spherical symmetry,  $\Omega_p^{(+)} = -\Omega_p^{(-)}$ , whenever  $S = 0$ , and it can be easily established from Eq. (28). But in the presence of the spin parameter, this is no longer valid as it can be interpreted from Fig. 5.

### B. Naked Kerr geometry

In this case, as shown in Figs. 6(a) and 6(b),  $\Omega_p$  explicitly depends on the sign of the spin parameter in the large limit. It is, in fact, related to the spin-spin coupling between the particle and the rotating spacetime. For a parallel arrangement, the force is repulsive, while it is attractive for the antiparallel situation. But the effect is only visible in the large limit such as  $S = -0.4M$ . For positive spin values, though, the nature almost remains similar to the geodesic case. But one can easily notice that for  $S \approx \mathcal{O}(M)$

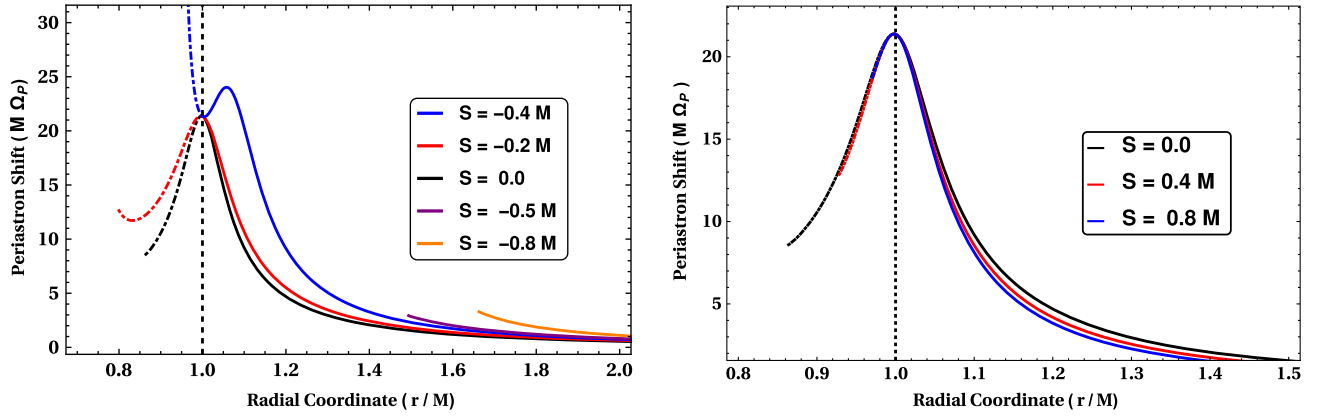
the timelike constraint as given in Eq. (17) will be particularly important, and this essentially restricts the motion close to singularity.

The effect of the sign of the spin parameter can be read off by investigating the nature of  $\Omega_\phi$  for positive and negative spin values. In the case of a negative spin,  $\Omega_\phi$  rapidly increases close to the singularity as a consequence of the attractive spin-spin force, as shown in Fig. 6(a). On the other hand, with a positive spin, the spin-spin force is repulsive, and  $\Omega_\phi$  slowly decreases close to the singularity similar to a geodesic orbit, depicted in Fig. 6(b). Even if this is the case for  $r \leq M$ , at  $r = M$ , the situation is different for nearly overspinning geometries as pointed out in Sec. IV C. The effect of the spin parameter is encoded within the term  $F(S)$  as shown in Eq. (33), and this can be easily neglected in the nearly overspinning limit. Though the analytic computation is carried out within the linear spin limit, it is true for any spin values as shown in Fig. 6. For example, at  $a = 1.001M$  and  $r = M$ , the value of  $M\Omega_p$  becomes 21.3614 in the  $S = 0$  limit, while for the  $S = 0.1M$  and  $S = -0.1M$  cases,  $M\Omega_p$  becomes 21.3631 and 21.3777 respectively.

For a consistency check, we compare our results with the periastron shift as given in Refs. [25,26]. In that case, an approximate expression for the ratio of angular frequency ( $\Omega_\phi$ ) and radial frequency ( $\Omega_r$ ) is given as

$$W_p = \frac{\Omega_\phi}{\Omega_r} = \left\{ 1 - \frac{6M}{r} + \frac{(8a + 6S)\sqrt{M}}{r^{3/2}} - \frac{3a^2 + 6aS}{r^2} - \frac{18M^{3/2}S}{r^{5/2}} + \frac{30MaS}{r^3} - \frac{12\sqrt{M}a^2S}{r^{7/2}} + \mathcal{O}(S^2) \right\}^{-1/2}, \quad (35)$$

where  $a$  and  $S$  are given as the spin parameters for the spacetime and the spinning particle respectively. A series



(a) The figure shows the frequency for large and negative spin values. For very large, such as  $S = -0.5M$  or  $S = -0.8M$ , the timelike constraint as given in Eq. (17) would be particularly important. Due to this, the particle may not be able to interact closely with the singularity. On the other hand, for  $S = -0.4M$ , the spin-spin interaction would play an important role as shown above.

(b) The nature of the plot does not alter by increasing (top to bottom) the spin value in the positive domain. It is easy to interpret that the timelike constraint as in Eq. (17) would be dominant in this limit.

FIG. 6. The periastron frequency is shown in an overspinning Kerr geometry with  $a = 1.001M$ .

expansion for the above formula to accommodate the leading order terms is given as

$$\Omega_P = 1 + \frac{3M}{r} - \frac{\sqrt{M}(4a + 3S)}{r^{3/2}} + \frac{3(9M^2 + a^2 + 2aS)}{2r^2} - \frac{3M^{3/2}}{r^{5/2}}(12aS + 6S) + \mathcal{O}(1/r^3). \quad (36)$$

Similarly, by employing Eq. (29), we also can establish

$$\frac{\Omega_\phi}{\Omega_r} = 1 + \frac{3M}{r} - \frac{\sqrt{M}(4a + 3S)}{r^{3/2}} + \frac{3(9M^2 + a^2 + 2aS)}{2r^2} - \frac{3M^{3/2}}{r^{5/2}}(12aS + 7S) + \mathcal{O}(1/r^3). \quad (37)$$

The above expression exactly matches with Eq. (36) up to the  $r^{-2}$  term, while from the term  $r^{-5/2}$  onward, the coefficients start to mismatch. This is due to the fact that they assume different sets of assumptions and techniques to evaluate the frequencies. More importantly, the angular velocity ( $\omega_\phi$ ) with respect to a static observer, i.e.,  $\omega_\phi = \frac{d\phi}{dt}$  given in Ref. [25], also follows an expression different from our approach.

## VI. CONCLUSION

In the present article, we have discussed the motion of a spinning particle in both overcharging Reissner-Nordström and overspinning Kerr spacetime. We primarily concentrated on the nearly circular orbits and computed the periastron precession related to them. For simplicity, we confined our computations within the equatorial plane and stuck to the linear approximation of the spin vector for

analytical convenience. Even if these calculations are proven to be useful in the  $S \ll \mathcal{O}(M)$  limit, to probe large spin values, one has to take into account the square order spin terms and also beyond that. Hence, a numerical evaluation is inevitable, and we carried out the same in our study.

We started with the Reissner-Nordström spacetime and studied the stable circular orbits for both geodesic and spinning particles. It was already pointed out in Ref. [47] that this is a nontrivial problem whenever one considers a naked singularity, i.e.,  $Q > M$ . Depending on the charge parameter of the spacetime, one may end up with two disconnected stable regions or a single smooth region. More precisely, for  $M < Q < Q_c$ , two disconnected regions appear, while for  $Q \geq Q_c$ , one comfortably gets a single and smooth stable region. The situation does not change radically as one considers a spinning particle instead of a geodesic. Only  $Q_c$  becomes a function of the spin parameter, and hence the regions of stability slightly change. Considering the precession frequency, one can easily show that critical charge parameter ( $Q_c^S$ ) explicitly affects the nature of  $\Omega_P$ . In the first case with two disconnected stable regions,  $\Omega_P$  steadily increases up to  $r = r_1^S$ , which is nothing but the ISCO. But in the second case,  $\Omega_P$  attains an extremal value in the stable domain as shown in Fig. 4. In the numerical analysis to probe large spin values, the situation remain similar to what is shown in Fig. 5.

Considering the second case with Kerr geometry, we first studied the stability of circular orbits on the equatorial plane. Though we particularly concentrated on the nearly overspinning limit as shown in Eq. (31), similar studies can be carried out for larger values of angular momentum of the spacetime. In the nearly overspinning limit, both the energy

and angular momentum approach zero at  $r \rightarrow M$ , which is true for any spin values. The periastron precession is shown in Fig. 6. It should be emphasized that spin-spin interaction between the rotating geometry and spinning particle will be crucial. This was particularly absent in case of the Reissner-Nordström spacetime. For large and negative spin values such as  $S = -0.4M$ , this force is attractive and is responsible for a large deviation as shown in Fig. 6. A further increase in the spin parameter ( $S = -0.8M$ ) essentially restricts the particle to interact closely with the singularity. This is due to the violation of the timelike constraint as shown in Eq. (17). We also pointed out that the effect of the spin parameter would be negligible at  $r \rightarrow M$  as far as one is working in the nearly overspinning limit. In addition, as one continues to make  $\epsilon$  smaller and smaller,  $\Omega_p$  corresponds to larger and larger values and eventually diverges for the  $\epsilon = 0$  limit. It is interesting to note that a similar

phenomenon can be shown in the case of energy extractions from a nearly overspinning geometry.

As we have already mentioned that the analysis is carried out completely on the equatorial plane for both the spacetimes, it would be a nontrivial exercise to carry out a similar study in the nonequatorial plane in the case of the Kerr geometry. We leave this as a future plan.

### ACKNOWLEDGMENTS

The author is indebted to Dr. Rajesh Kumble Nayak for fruitful discussions on numerous occasions. He is also thankful to the Visiting Associateship programme of Inter-University Centre for Astronomy and Astrophysics (IUCAA), Pune. A part of this work was carried out during a visit to IUCAA under this programme. Finally, the author wish to thank the respected reviewer for useful comments and suggestions to improve the manuscript.

- 
- [1] E. Barausse and A. Buonanno, Improved effective-one-body Hamiltonian for spinning black-hole binaries, *Phys. Rev. D* **81**, 084024 (2010).
  - [2] A. Taracchini *et al.*, Effective-one-body model for black-hole binaries with generic mass ratios and spins, *Phys. Rev. D* **89**, 061502 (2014).
  - [3] E. Barausse and A. Buonanno, Extending the effective-one-body Hamiltonian of black-hole binaries to include next-to-next-to-leading spin-orbit couplings, *Phys. Rev. D* **84**, 104027 (2011).
  - [4] S.N. Rasband, Black Holes and Spinning Test Bodies, *Phys. Rev. Lett.* **30**, 111 (1973).
  - [5] S. Suzuki and K.-i. Maeda, Innermost stable circular orbit of a spinning particle in Kerr space-time, *Phys. Rev. D* **58**, 023005 (1998).
  - [6] T. A. Apostolatos, A spinning test body in the strong field of a schwarzschild black hole, *Classical Quantum Gravity* **13**, 799 (1996).
  - [7] O. Semerák and M. Šrámek, Spinning particles in vacuum spacetimes of different curvature types, *Phys. Rev. D* **92**, 064032 (2015).
  - [8] M. Mathisson, Neue mechanik materieller systemes, *Acta Phys. Pol.* **6**, 163 (1937).
  - [9] A. Papapetrou, Spinning test particles in general relativity. 1, *Proc. R. Soc. A* **209**, 248 (1951).
  - [10] E. Corinaldesi and A. Papapetrou, Spinning test-particles in general relativity. 2, *Proc. R. Soc. A* **209**, 259 (1951).
  - [11] W. Dixon, A covariant multipole formalism for extended test bodies in general relativity, *Nuovo Cimento* **34**, 317 (1964).
  - [12] W.G. Dixon, Dynamics of extended bodies in general relativity. i. Momentum and angular momentum, *Proc. R. Soc. A* **314**, 499 (1970).
  - [13] W.G. Dixon, Dynamics of extended bodies in general relativity iii. Equations of motion, *Phil. Trans. R. Soc. A* **277**, 59 (1974).
  - [14] M. D. Hartl, A survey of spinning test particle orbits in Kerr space-time, *Phys. Rev. D* **67**, 104023 (2003).
  - [15] W. Han, Chaos and dynamics of spinning particles in Kerr spacetime, *Gen. Relativ. Gravit.* **40**, 1831 (2008).
  - [16] Y. Pan, A. Buonanno, A. Taracchini, L. E. Kidder, A. H. Mrou, H. P. Pfeiffer, M. A. Scheel, and B. Szilgyi, Inspiral-merger-ringdown waveforms of spinning, precessing black-hole binaries in the effective-one-body formalism, *Phys. Rev. D* **89**, 084006 (2014).
  - [17] E. Barausse, E. Racine, and A. Buonanno, Hamiltonian of a spinning test-particle in curved spacetime, *Phys. Rev. D* **80**, 104025 (2009); Erratum, *Phys. Rev. D* **85**, 069904 (2012).
  - [18] J. Vines, D. Kunst, J. Steinhoff, and T. Hinderer, Canonical Hamiltonian for an extended test body in curved spacetime: To quadratic order in spin, *Phys. Rev. D* **93**, 103008 (2016).
  - [19] R. Schodel *et al.*, A star in a 15.2 year orbit around the supermassive black hole at the center of the Milky Way, *Nature (London)* **419**, 694 (2002).
  - [20] A. Hees *et al.*, Testing General Relativity with Stellar Orbits around the Supermassive Black Hole in Our Galactic Center, *Phys. Rev. Lett.* **118**, 211101 (2017).
  - [21] E. V. Pitjeva, Relativistic effects and solar oblateness from radar observations of planets and spacecraft, *Astron. Lett.* **31**, 340 (2005).
  - [22] J.P. Rozelot and C. Damiani, History of solar oblateness measurements and interpretation, *Eur. Phys. J. H* **36**, 407 (2011).
  - [23] A. Einstein, Erklärung der perihelionbewegung der merkur aus der allgemeinen relativitätstheorie, *Sitzungsber. Preuss. Akad. Wiss. Phys. Math. Kl.* **47**, 831 (1915).

- [24] E. Hackmann, C. Lmmerzahl, Y. N. Obukhov, D. Puetzfeld, and I. Schaffer, Motion of spinning test bodies in Kerr spacetime, *Phys. Rev. D* **90**, 064035 (2014).
- [25] T. Hinderer *et al.*, Periastron advance in spinning black hole binaries: Comparing effective-one-body and Numerical Relativity, *Phys. Rev. D* **88**, 084005 (2013).
- [26] A. Le Tiec *et al.*, Periastron advance in spinning black hole binaries: Gravitational self-force from numerical relativity, *Phys. Rev. D* **88**, 124027 (2013).
- [27] T. Damour, P. Jaranowski, and G. Schaefer, Dynamical invariants for general relativistic two-body systems at the third post-Newtonian approximation, *Phys. Rev. D* **62**, 044024 (2000).
- [28] M. D. Hartl and A. Buonanno, The dynamics of precessing binary black holes using the post-Newtonian approximation, *Phys. Rev. D* **71**, 024027 (2005).
- [29] A. Gopakumar and C. Konigsdorffer, The deterministic nature of conservative post-Newtonian accurate dynamics of compact binaries with leading order spin-orbit interaction, *Phys. Rev. D* **72**, 121501 (2005).
- [30] G. Faye, L. Blanchet, and A. Buonanno, Higher-order spin effects in the dynamics of compact binaries. I. Equations of motion, *Phys. Rev. D* **74**, 104033 (2006).
- [31] L. E. Kidder, Coalescing binary systems of compact objects to post-Newtonian 5/2 order. 5. Spin effects, *Phys. Rev. D* **52**, 821 (1995).
- [32] G. W. Gibbons, S. A. Hartnoll, and A. Ishibashi, On the stability of naked singularities, *Prog. Theor. Phys.* **113**, 963 (2005).
- [33] C. Chakraborty, M. Patil, P. Kocherlakota, S. Bhattacharyya, P. S. Joshi, and A. Krlak, Distinguishing Kerr naked singularities and black holes using the spin precession of a test gyro in strong gravitational fields, *Phys. Rev. D* **95**, 084024 (2017).
- [34] F. de Felice, Repulsive phenomena and energy emission in the field of a naked singularity, *Astron. Astrophys.* **34**, 15 (1974).
- [35] F. de Felice, Classical instability of a naked singularity, *Nature (London)* **273**, 429 (1978).
- [36] M. Patil and P. S. Joshi, Kerr naked singularities as particle accelerators, *Classical Quantum Gravity* **28**, 235012 (2011).
- [37] G. Dotti, R. Gleiser, and J. Pullin, Instability of charged and rotating naked singularities, *Phys. Lett. B* **644**, 289 (2007).
- [38] S. Chandrasekhar, *The Mathematical Theory of Black Holes* (Oxford University, New York, 1998), Vol. 69.
- [39] S. W. Hawking and G. F. R. Ellis, *The Large Scale Structure of Space-Time* (Cambridge University Press, Cambridge, England, 1973), Vol. 1.
- [40] R. Penrose, Gravitational Collapse and Space-Time Singularities, *Phys. Rev. Lett.* **14**, 57 (1965).
- [41] W. Tulczyjew, Motion of multipole particles in general relativity theory, *Acta Phys. Pol.* **18**, 393 (1959).
- [42] O. Semerak, Spinning test particles in a Kerr field. 1., *Mon. Not. R. Astron. Soc.* **308**, 863 (1999).
- [43] M. Saijo, K.-i. Maeda, M. Shibata, and Y. Mino, Gravitational waves from a spinning particle plunging into a Kerr black hole, *Phys. Rev. D* **58**, 064005 (1998).
- [44] R. Rudiger, Conserved quantities of spinning test particles in general relativity. i, *Proc. R. Soc. A* **375**, 185 (1981).
- [45] R. Rudiger, Conserved quantities of spinning test particles in general relativity. ii, *Proc. R. Soc. A* **385**, 229 (1983).
- [46] P. I. Jefremov, O. Yu. Tsupko, and G. S. Bisnovaty-Kogan, Innermost stable circular orbits of spinning test particles in Schwarzschild and Kerr space-times, *Phys. Rev. D* **91**, 124030 (2015).
- [47] D. Pugliese, H. Quevedo, and R. Ruffini, Circular motion of neutral test particles in Reissner-Nordström spacetime, *Phys. Rev. D* **83**, 024021 (2011).
- [48] J. M. Bardeen, W. H. Press, and S. A. Teukolsky, Rotating black holes: Locally nonrotating frames, energy extraction, and scalar synchrotron radiation, *Astrophys. J.* **178**, 347 (1972).
- [49] B. O'Neil, *The geometry of kerr black holes* (A K Peters, Wellesley, Massachusetts, 1995).
- [50] G. Preti and F. d. Felice, Light cones and repulsive gravity, *Am. J. Phys.* **76**, 671 (2008).
- [51] O. Luongo and H. Quevedo, in *Toward an invariant definition of repulsive gravity*, edited by T. Damour, R. T. Jantzen, and R. Ruffini *Proceedings of the 12th Marcel Grossmann Meeting on General Relativity* (World Scientific, Singapore, 2010), Vols. 1–3, p. 1029.
- [52] R. M. Wald, *General Relativity* (University of Chicago, Chicago, 2010).
- [53] M. Patil and P. S. Joshi, Finite escape fraction for ultrahigh energy collisions around Kerr naked singularity, *Pramana* **84**, 491 (2015).
- [54] M. Patil, T. Harada, K.-i. Nakao, P. S. Joshi, and M. Kimura, Infinite efficiency of the collisional Penrose process: Can an overspinning Kerr geometry be the source of ultrahigh-energy cosmic rays and neutrinos?, *Phys. Rev. D* **93**, 104015 (2016).